Available online at www.sciencedirect.com
ScienceDirect
International Journal of Solids and Structures 43 (2006) 6630–6648
INTERNATIONAL JOURNAL OF SOLIDS and STRUCTURES
www.elsevier.com/locate/ijsolstr

Cohesive zone model of intermediate crack-induced debonding of FRP-plated concrete beam

Jialai Wang *

Department of Civil, Construction, and Environmental Engineering, The University of Alabama, Tuscaloosa, AL 35487-0205, USA

Received 31 May 2005; received in revised form 26 December 2005
Available online 31 March 2006

Abstract

External bonding of FRP plates or sheets has emerged as a popular method for strengthening reinforced concrete structures. Debonding along the FPR–concrete interface can lead to premature failure of the structures. In this study, debonding induced by a flexural crack in a FRP-plated concrete beam is analyzed through a nonlinear fracture mechanics method. The concrete beam and FRP plate are modeled as linearly elastic simple beams connected together through a thin layer of FRP–concrete interface. A bi-linear cohesive (bond-slip) law, which has been verified by experiments, is used to model the FRP–concrete interface as a cohesive zone. Thus a cohesive zone model for intermediate crack-induced debonding is established with a unique feature of unifying the debonding initiation and growth into one model. Closed-form solutions of interfacial stress, FRP stress and ultimate load of the plated beam are obtained and then verified with the numerical solutions based on finite element analysis. Parametric studies are carried out to demonstrate the significant effect of FRP thickness on the interface debonding. The bond-slip shape is examined specifically. In spite of its profound effect on softening zone size, the bond-slip shape has been found to have little effect on the ultimate load of the plated beam. By making use of such a unique feature, a simplified explicit expression is obtained to determine the ultimate load of the plated concrete beam with a flexural crack conveniently. The cohesive zone model in this study also provides an efficient and effective way to analyze more general FRP–concrete interface debonding.

Keywords: Cohesive zone model; Fiber reinforced polymer; Strengthening; Concrete; Debonding

1. Introduction

External bonding of FRP plates or sheets has emerged as a popular method for strengthening conventional materials such as reinforced concrete. The interface between the FRP and concrete plays a critical role in this strengthening method by providing effective stress transfer from the existing structures to externally bonded FRP plates or sheets and keeping integrity and durability of the composite performance of FRP–concrete hybrid structures. Debonding along the FPR-concrete interface can lead to premature failure of the structure.

* Tel.: +1 205 348 6786; fax: +1 205 348 0783.
E-mail address: jwang@eng.ua.edu

0020-7683/$ - see front matter © 2006 Elsevier Ltd. All rights reserved.
doi:10.1016/j.ijsolstr.2006.01.013

Here, the FRP–concrete interface refers to a thin layer of adhesive and the adjacent concrete within which the relative deformation between FRP and concrete mainly happens as revealed by experiment study (Yuan et al., 2004). Therefore, the debonding of the FRP–concrete interface has to be properly characterized and modeled before this technique can be commonly accepted in practice.

FRP–concrete interface debonding can be generally classified into two major types (Teng et al., 2003): plate end debonding and intermediate crack-induced debonding (IC debonding). The former debonding model has been studied extensively in the last decades (Roberts and Haji-Kazemi, 1989; Malek and Saadatmanesh, 1998; Smith and Teng, 2001); while only a few studies have been conducted on the latter mode. Wu et al. (1997) took an experimental and numerical combined approach to study IC debonding. They tested a plain concrete beam reinforced by FRP plate under three-point bending load on which a mid-span notch was created to simulate a mid-span crack. Later, they also developed a fracture mechanics based model (Yuan et al., 2001) to analyze IC debonding. The significance of IC debonding was also examined experimentally by Sebastian (2001). To provide quantitative stress distribution at the vicinity of the intermediate crack, Leung (2001) developed a linear fracture mechanics solution in which a linear elastic model was used to model the FRP–concrete interface. This linear elastic model of interface was also adopted by others (Neubauer and Rostasy, 1999; Lau et al., 2001; Rabinovitch and Frostig, 2001) in studying cracked concrete beams flexurally reinforced by FRP composites. A strength model of IC debonding was proposed by Teng et al. (2003) recently.

Although the linear elastic model is used conveniently in the literature to model IC debonding, experimental studies have shown that the real stress deformation relationship of the FRP–concrete interface is nonlinear (Chajes et al., 1995, 1996; Bizindavyi and Neale, 1999; Dai et al., 2005; Yao et al., 2005). The stress deformation relationship is generally referred to as bond-slip law in the literature since the deformation of interface is mainly the relative displacement (slip) between the FRP plate and the concrete beam. Generally, this nonlinear relationship consists of two stages: an initially elastic stage in which the interfacial stress increases with the slip until it reaches a maximum value, and a softening stage in which the interfacial stress decreases with the slip. Existing solutions of IC debonding fail to consider the softening stage of the interface and therefore, are limited to elastic analysis and cannot be used to simulate debonding growth. By considering a nonlinear bond-slip law, it is possible to model the whole debonding process of FRP–concrete interface as demonstrated recently by Yuan et al. (2004). Existing solutions of such an approach are limited to simple single-lag shear specimen (Triantafillou and Plevris, 1992; Taljsten, 1996, 1997; Yuan et al., 2001; Wu et al., 2002a,b; Yuan et al., 2004). With aim to efficiently simulate and better understand the IC debonding behavior, an analytical model by using a nonlinear bond-slip law is developed for the FRP-reinforced concrete beam in this study.

As much experimental evidence (Chajes et al., 1995, 1996; Bizindavyi and Neale, 1999; Taljsten, 1997) shows, the interface defined previously can be viewed as a large-scale fracture process zone (cohesive zone). The nonlinear bond-slip relationship essentially is the cohesive law of this zone. Therefore, by using a nonlinear bond-slip law in the analytical model, the debonding process is essentially approached through a non-linear fracture mechanics method—cohesive zone model (CZM). Cohesive zone model (CZM) pioneered by Dugdale (1960) and Barenblatt (1962) is gaining more and more attention and popularity nowadays in modeling fracture processes with large-scale fracture process zones. In CZM, the locally damaged materials forming a narrow band of localized deformation may be modeled by nonlinear springs which represent the major physical variables. Compared with the single-parameter fracture approach of linearly elastic fracture mechanics, which ignores the microscopic details and discloses little what happens within the damage zone, the CZM takes the behavior of fracture processing zone into consideration and provides a way to examine the "inner problem" of understanding, characterizing and modeling the failure processes that actually lead to energy dissipation. What is more, the CZM unifies the crack initiation and growth into one model and can be easily formulated and implemented in numerical simulation, such as the "interface element" method in finite element code (Yan et al., 2001; Blackman et al., 2003).

In this study, a cohesive zone model of IC debonding along the FRP–concrete interface is established analytically by using a non-linear bond-slip law. This paper is arranged as follows: the closed-form solution of the cohesive zone model for IC debonding is first established, followed by a case study of midspan debonding of a FRP-plated beam under point load. Parametric study is then carried out to study the effects of FRP stiffness and bond-slip shape on the IC debonding of the FRP–concrete interface.

2. Cohesive zone model of IC debonding

2.1. Bi-beam system

Consider a simply-supported reinforced concrete beam (RC beam) reinforced by an FRP plate subjected to point loads and/or uniform distributed load, as shown in Fig. 1(a). To simplify the analysis, only a flexural crack existing at the mid-span of the concrete beam is considered in this study. For more general configurations of cracked beams, similar procedure as developed next can be used. Since a symmetric load is applied, only half of the structure needs to be analyzed (Fig. 1(b)). The geometry of the cross-section of the plated beam is shown in Fig. 1(a). Similar to many other researchers (Roberts and Haji-Kazemi, 1989; Malek and Saadatmanesh, 1998; Smith and Teng, 2001), both the concrete beam and the FRP plate are modeled as linear elastic simple beams (beam 1 and 2 in Fig. 1, respectively). Therefore, the constitutive laws for these two beams read:

$$N_i = C_i u_i', \quad M_i = -D_i w_i'', \quad i = 1, 2 \tag{1}$$

where N_i and M_i are axial forces and bending moments of beam i ($i = 1, 2$), respectively; u_i and w_i are axial and vertical displacements of beam i ($i = 1, 2$), respectively; C_i and D_i are axial and bending stiffnesses of beam i ($i = 1, 2$), respectively; and $C_i = E_i b_i h_i$, $D_i = E_i I_i$; E_i is the Young's modulus of beam i ($i = 1, 2$); b_i and h_i are width and height of beam i ($i = 1, 2$); I_i is the moment of inertia of the beam i ($i = 1, 2$).

It should be pointed out that such a model is a simplification of a real FRP-plated RC beam in which the RC beam is not strictly linearly elastic and there are usually more than one flexural cracks existing. Nevertheless, the model in this study allows us to obtain simple closed-form solutions of IC debonding, and can be extended to more complicated cases in which the nonlinearity of concrete behavior and multiple cracks are considered. New lights can also be shed on the IC debonding process and the significant effect of bond-slip on IC debonding.

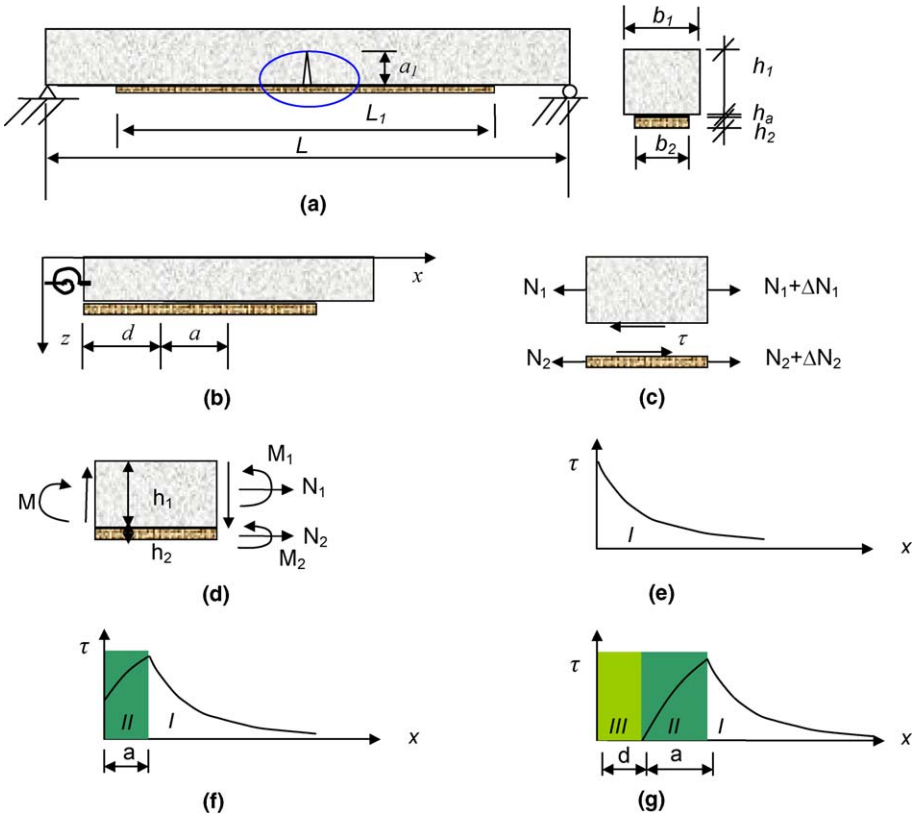

Fig. 1. Interfacial stress of a FRP-plated concrete beam with a mid-span crack.

The flexural crack introduces local flexibility at the crack location and is conventionally modeled as a rotational spring with infinitesimal thickness at the crack location (Fig. 1(b)). For a plain concrete beam, if the depth of the crack is known, the rotational stiffness of the spring K_r can be estimated by (Paipetis and Dimarogonas, 1986):

$$K_r = c(a_1, h_1)D_1 \tag{2}$$

where h_1 and a_1 are the thickness of the beam, the depth of the crack, respectively; D_1 is the bending stiffness of the whole concrete beam at the location of the crack, and $c(a_1, h_1)$ is determined by the crack geometry. Based on fracture mechanics principles, for example, $c(a_1, h_1)$ can be approximated for $a_1/h_1 < 0.6$ as (Paipetis and Dimarogonas, 1986):

$$c(a_1,h_1) = \frac{1}{5.346h_1}\left(1.8624\left(\frac{a_1}{h_1}\right)^2 - 3.95\left(\frac{a_1}{h_1}\right)^3 + 16.375\left(\frac{a_1}{h_1}\right)^4 - 37.226\left(\frac{a_1}{h_1}\right)^5 + 76.81\left(\frac{a_1}{h_1}\right)^6 - 126.9\left(\frac{a_1}{h_1}\right)^7 + 172\left(\frac{a_1}{h_1}\right)^8 - 143.97\left(\frac{a_1}{h_1}\right)^9 + 66.56\left(\frac{a_1}{h_1}\right)^{10}\right)^{-1} \tag{3}$$

However, it is difficult to obtain an explicit expression of K_r for RC beam due to the existence of steel bars. In such a case, a trial-and-error method proposed by Rabinovitch and Frostig (2001) has to be used.

Considering the free body diagram of Fig. 1(c) and (d), equilibrium equations on axial direction and bending moment can be obtained as

$$\frac{dN_1}{dx} = b_2\tau, \quad \frac{dN_2}{dx} = -b_2\tau \tag{4}$$

$$M = M_1 + M_2 + N_2(Y_1 + Y_2) \tag{5}$$

where τ is the interfacial shear stress. Y_1 and Y_2 are the distances from the bottom of beam 1 and the top of beam 2 to their respective neutral axis.

It should be pointed out that interfacial normal (peel) stress also exists. It is not shown in Fig. 1(c) and considered in this study for the following reasons. (a) Existing solutions (Smith and Teng, 2001) show that the normal stress has little effect on the derivation of shear stress. (b) According to Rabinovitch and Frostig (2001), the concrete beam and FRP plate are in contact at the vicinity of the flexural crack. This suggests that the normal interface stress is compressive at this location and, therefore, doesn't affect the debonding of the FRP–concrete interface if fiction is neglected. This is different from the normal stress at the FRP plate end, which is tensile and plays a critical role in the plate end debonding. (c) Strictly speaking, any interface fracture is naturally mixed-moded (Hutchinson and Suo, 1992) and the stress status within the interface layer is very complicated. Nevertheless, for a given shearing fracture energy introduced on the debonding surface, the mode I and mode II fracture energy values can be linearly related, as found by Wu et al. (2002a,b). In such a way, the IC debonding can be treated approximately as a mode II fracture (Yuan et al., 2004; Niu and Wu, 2005).

Beam 2 is bonded to Beam 1 through the FRP–concrete interface layer which is modeled as a large fracture process zone with a nonlinear bond-slip law as demonstrated in many experimental studies (Chajes et al., 1995, 1996; Bizindavyi and Neale, 1999). It has been shown by experiments (Wu and Yin, 2003; Nakaba et al., 2001) that a bi-linear bond-slip relationship in Fig. 2 can be a good approximation of this non-linear relationship. In Fig. 2, the bond-slip law has three segments: (1) elastic stage when $\tau \leqslant \tau_f$ or $\delta \leqslant \delta_1$: stress increases linearly with slip; (2) softening stage when $\delta_1 < \delta \leqslant \delta_f$: stress decreases linearly with slip; and (3) debonding stage when $\delta_f \leqslant \delta$: stress is zero and FRP is separated from the concrete beam. This non-linear relationship can be described by the following equation:

$$\tau = \begin{cases} \dfrac{\tau_f}{\delta_1}\delta & 0 \leqslant \delta \leqslant \delta_1 \\ \dfrac{\delta_f - \delta}{\delta_f - \delta_1}\tau_f & \delta_1 \leqslant \delta \leqslant \delta_f \\ 0 & \delta > \delta_f \end{cases} \tag{6}$$

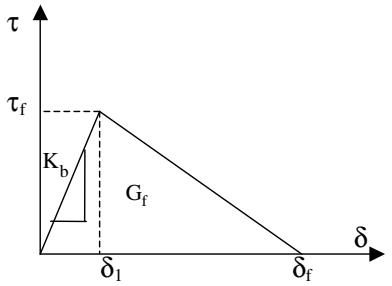

Fig. 2. Bi-linear bond-slip model.

where δ is the slip along the interface (relative axial displacement of the top of the FRP plate and the bottom of the concrete beam) and given by

$$\delta = \left(u_1 - Y_1 w_1' - u_2 - Y_2 w_2'\right) \tag{7}$$

From the point of view of CZM, such a nonlinear relationship is a material property of the FRP–concrete interface. τ_f is the shear strength of the interface; δ_f is the separation slip; $K_b = \tau_f/\delta_1$ is the initial elastic stiffness of the FRP–concrete interface; and the area given by the area under the curve is the fracture energy G_f which can be calculated by

$$G_f = \int_0^{\delta_f} \tau \, d\delta = \frac{1}{2}\delta_f \tau_f \tag{8}$$

The above bond-slip model implies that the shear stress is constant along the thickness direction within the interface layer. This is a simplification of the complex stress variation of the interface stresses in that direction. One drawback to this model is that the boundary condition of shear stress at the location of the flexural crack and the plate end (where $\tau = 0$) cannot be satisfied. However, such a simplification only affects the shear stress at a very small region at the vicinity of the crack and plate end. Therefore, the bond-slip model is widely adopted to obtain interfacial stress of FRP-plated beams (Roberts and Haji-Kazemi, 1989; Malek and Saadatmanesh, 1998; Smith and Teng, 2001).

2.2. Debonding analysis

Under external load, interfacial shear stress is developed along the FRP–concrete interface. Initially, the applied load is small and the maximum interfacial stress τ is less than τ_f and therefore, the interface is in its elastic stage. The interfacial shear stress distribution at this stage can be sketched as shown in Fig. 1(e). Due to the crack tip opening displacement introduced by the flexural crack, a finite slip between the FRP plate and the concrete beam exists at the location of the crack. A stress concentration is introduced by this slip at the vicinity of the flexural crack. This stage ends when the interfacial stress reaches τ_f or the slip reaches δ_1. If we keep on increasing the load, the slip at the location of the flexural crack becomes greater than δ_1 and the FRP–concrete interface begins to linearly soften with the slip. This is an elastic-softening stage in which two distinct regions appear along the interface as shown in Fig. 1(f). In region I, the slip is less than δ_1 and the interface is linearly elastic; while in region II, the slip is greater than δ_1 and the shear stress reduces linearly. If the slip at the location of the crack is greater than the separation slip δ_f, shear stress reduces to zero and full debonding initiates and grows along the FRP–concrete interface which forms region III, a fully debonded region.

2.2.1. Stage I: Linearly elastic stage

In this stage, the bond-slip relation is given by the first equation of Eq. (6). Substituting Eq. (7) into this equation yields

$$\tau = \frac{\tau_f}{\delta_1}\left(u_1 - Y_1 w_1' - u_2 - Y_2 w_2'\right) \tag{9}$$

Differentiating both sides of Eq. (9) with respect to x gives

$$\tau' = \frac{\tau_f}{\delta_1}\left(u_1' - Y_1 w_1'' - u_2' - Y_2 w_2''\right) \tag{10}$$

An assumption used commonly in the literature (Smith and Teng, 2001; Rasheed and Pervaiz, 2002) is adopted in this study, which states that the FRP plate and concrete beam have the same curvature, i.e.,

$$w_1'' = w_2'' \tag{11}$$

Substituting Eq. (11) and constitutive equation (1) into Eq. (5), we have

$$w_1'' = -\frac{M}{D_1 + D_2} + \frac{Y_1 + Y_2}{D_1 + D_2} N_2 \tag{12}$$

Substituting Eq. (12) into Eq. (10) and considering Eq. (1), we obtain

$$\tau' = \frac{\tau_f}{\delta_1}\left(\frac{N_1}{C_1} - \frac{N_2}{C_2} + \frac{Y_1 + Y_2}{D_1 + D_2}(M - (Y_1 + Y_2)N_2)\right) \tag{13}$$

Differentiating both sides of Eq. (13) with respect to x and considering equilibrium equation Eq. (5) give the governing equation of shear stress along the interface of FRP and concrete:

$$\tau'' = \frac{\tau_f}{\delta_1}\left(\frac{1}{C_1} + \frac{1}{C_2} + \frac{(Y_1 + Y_2)^2}{(D_1 + D_2)}\right) b_2 \tau + \frac{\tau_f}{\delta_1}\frac{Y_1 + Y_2}{D_1 + D_2} M' \tag{14}$$

The solution can be expressed as

$$\tau = A e^{-\lambda_1 x} + B e^{\lambda_1 x} + \tau_C \tag{15}$$

where

$$\lambda_1 = C_\lambda \sqrt{\frac{\tau_f}{\delta_1}}, \quad \tau_C = C_\tau M', \quad C_\lambda = \sqrt{b_2\left(\frac{1}{C_1} + \frac{1}{C_2} + \frac{(Y_1 + Y_2)^2}{D_1 + D_2}\right)}, \quad C_\tau = \frac{Y_1 + Y_2}{(D_1 + D_2)C_\lambda^2} \tag{16}$$

τ_C is the particular solution of Eq. (14) and essentially the shear stress along the FRP–concrete interface if the FRP–concrete system is treated as a fully composite beam. Noting that when x is sufficient large, shear stress is limited and converges to its particular solution, $B = 0$ (Wang and Qiao, 2004). The axial force in the FRP plate can be obtained through Eq. (4) as

$$N_2 = N_{20} + \int_0^x b_2(\Delta\tau + \tau_C)\,dx = N_{20} - \int_0^x b_2(A e^{-\lambda_1 x} + \tau_C)\,dx = N_{2C} + \Delta N_2 \tag{17}$$

where

$$N_{2C} = \int_x^{L/2} b_2 C_\tau M'\,dx = -b_2 C_\tau M \tag{18}$$

$$\Delta N_2 = N_{20} - \int_0^x b_2 A e^{-\lambda_1 x}\,dx - b_2 \int_0^{L/2} C_\tau M'\,dx = N_{20} - N_{2C0} - b_2 \frac{A}{\lambda_1}(1 - e^{\lambda_1 x}) \tag{19}$$

where N_{2C} is the axial force of the FRP plate if the FRP–concrete system is treated as a fully composite beam and

$$N_{2C0} = N_{2C}|_{x=0} = -b_2 C_\tau M|_{x=0} \tag{20}$$

At locations sufficiently far away from the crack, the axial force in the FRP plate is reduced to the composite beam solution. Considering Eq. (17), we have

$$N_{20} = N_{2C0} + b_2 \frac{A}{\lambda_1} \tag{21}$$

$$\Delta N_2 = \frac{b_2 A}{\lambda_1} e^{-\lambda_1 x} \tag{22}$$

To determine A, displacement boundary condition at $x = 0$ is employed. Considering the symmetry, the displacement boundary condition is given by

$$w_1'|_{x=0} = -\frac{M_1|_{x=0}}{2K_r} \tag{23}$$

The bond slip at the location of the flexural crack is then obtained as

$$\delta|_{x=0} = \delta_1 = \left(u_1 - Y_1 w_1' - u_2 - Y_2 w_2'\right)\big|_{x=0} = \left.\frac{Y_1}{2K_r} M_1\right|_{x=0} \tag{24}$$

According to Eq. (12), we have

$$M_1|_{x=0} = \left.\frac{D_1}{D_1 + D_2}(1 + (Y_1 + Y_2)b_2 C_\tau)M\right|_{x=0} - \frac{D_1(Y_1 + Y_2)}{D_1 + D_2}\frac{Ab_2}{\lambda_1} \tag{25}$$

Substituting Eqs. (24), (21), (22), (15) into (9) at $x = 0$, A is determined as

$$A = \frac{\frac{\tau_f}{\delta_1}\frac{Y_1}{2K_r}\frac{D_1}{D_1+D_2}(1 + (Y_1 + Y_2)b_2 C_\tau)M|_{x=0} - \tau_C|_{x=0}}{1 + \frac{\tau_f}{\delta_1}\frac{Y_1}{2K_r}\frac{D_1}{D_1+D_2}(Y_1 + Y_2)\frac{b_2}{\lambda_1}} \tag{26}$$

The interface shear stress presented by Eq. (15) increases linearly with the applied load until it reaches the shear limit τ_f, i.e.

$$\tau|_{x=0} = \tau_f \tag{27}$$

Substituting Eq. (26) into Eq. (27), we can solve the elastic limit which is the maximum load under which the interface is under elastic stage.

2.2.2. Stage II: Elastic-softening stage

If the load is increased after reaching the elastic limit, part of the interface turns to soften with the slip and two regions along the interface are formed (Fig. 1(f)).

2.2.2.1. Region I: Linearly elastic region ($\delta \leqslant \delta_1$). In this region, solution of shear stress has the same form as in Eq. (15)

$$\tau = A_1 e^{-\lambda_1(x-a)} + \tau_C \tag{28}$$

where a is the softening zone size and coefficient A_1 is determined by the boundary condition:

$$\tau|_{x=a} = \tau_f \tag{29}$$

Therefore, A_1 is obtained as

$$A_1 = \tau_f - \tau_C|_{x=a} \tag{30}$$

Similar to the previous section, the axial force in this region can be obtained as

$$N_{2e} = N_{2C} + \Delta N_{2e}, \quad \Delta N_{2e} = \frac{b_2(\tau_f - \tau_C|_{x=0})}{\lambda_1} e^{-\lambda_1(x-a)} \tag{31}$$

2.2.2.2. Region II: Linearly softening region ($\delta_1 < \delta \leqslant \delta_f$). Considering the second expression of bond-slip relation in Eq. (6), Eq. (10) turns to

$$\tau' = \frac{-\tau_f}{\delta_f - \delta_1}\left(u_1' - Y_1 w_1'' - u_2' - Y_2 w_2''\right) \tag{32}$$

Differentiating both sides of Eq. (32) with respect to x again, we have

$$\tau'' = \frac{-\tau_f}{\delta_f - \delta_1}\left(\frac{1}{C_1} + \frac{1}{C_2} + \frac{(Y_1 + Y_2)^2}{D_1 + D_2}\right)b_2\tau - \frac{\tau_f}{\delta_f - \delta_1}\frac{Y_1 + Y_2}{D_1 + D_2}M' \tag{33}$$

The solution of Eq. (33) is then obtained as

$$\tau = C\cos(\lambda_2(x-a)) + D\sin(\lambda_2(x-a)) + \tau_C \tag{34}$$

and

$$\lambda_2^2 = \frac{\tau_f}{\delta_f - \delta_1}\left(\frac{1}{C_1} + \frac{1}{C_2} + \frac{(Y_1+Y_2)^2}{D_1+D_2}\right) = \frac{\delta_1}{\delta_f - \delta_1}\lambda_1^2 \tag{35}$$

C and D are two coefficients determined by continuous conditions at $x = a$

$$\tau|_{x=a-} = \tau_f, \quad \tau'|_{x=a-} = -\frac{\delta_1}{\delta_f - \delta_1}\tau'\Big|_{x=a+} \tag{36}$$

Substituting the shear stress solution Eq. (34) into above continuous equations, we can determine C and D as

$$C = \tau_f - \tau_C|_{x=a}, \quad D = \frac{\lambda_2}{\lambda_1}(\tau_f - \tau_C|_{x=a}) - \frac{1}{\lambda_2}\frac{\delta_f}{\delta_f - \delta_1}\tau_C'\Big|_{x=a} \tag{37}$$

Axial force of the FRP plate in this region is then calculated based on the constitutive law Eq. (1):

$$N_{2S} = N_{20} - b_2\int_0^x (C\cos(\lambda_2(x-a)) + D\sin(\lambda_2(x-a)) + \tau_C)\,dx = N_{2C} + \Delta N_{2S} \tag{38}$$

where

$$\Delta N_{2S} = N_{20} - N_{2C0} - \frac{b_2}{\lambda_2}(C(\sin(\lambda_2 a) + \sin(\lambda_2(x-a))) - D(\cos(\lambda_2(x-a)) - \cos(\lambda_2 a))) \tag{39}$$

Considering the continuous condition of the axial force at $x = a$, we have

$$\Delta N_{2S}|_{x=a} = \frac{b_2(\tau_f - \tau_C|_{x=a})}{\lambda_1} \tag{40}$$

Hence

$$N_{20} = N_{2C0} + \frac{b_2}{\lambda_2}\left(\sin(\lambda_2 a) + \frac{\lambda_2}{\lambda_1}\cos(\lambda_2 a)\right)(\tau_f - \tau_C|_{x=a}) + \frac{b_2}{\lambda_2^2}\frac{\delta_f}{\delta_f - \delta_1}(1 - \cos(\lambda_2 a))\tau_C'\Big|_{x=a} \tag{41}$$

and

$$\Delta N_{2S} = \frac{b_2}{\lambda_2}\left(\sin(\lambda_2(a-x)) - \frac{\lambda_2}{\lambda_1}\cos(\lambda_2(a-x))\right) + \frac{b_2}{\lambda_2^2}\frac{\delta_f}{\delta_f - \delta_1}(1 - \cos(\lambda_2(x-a)))\tau_C'\Big|_{x=a} \tag{42}$$

Considering the shear stress at $x = 0$:

$$\Delta N_{2S} = -\frac{b_2}{\lambda_2}\left(\sin(\lambda_2(x-a)) - \frac{\lambda_2}{\lambda_1}\cos(\lambda_2(x-a))\right)(\tau_f - \tau_C|_{x=a}) + \frac{b_2}{\lambda_2^2}\frac{\delta_f}{\delta_f - \delta_1}(1 - \cos(\lambda_2(x-a)))\tau_C'\Big|_{x=a} \tag{43}$$

Substituting Eqs. (24), (34), (37) into Eq. (43) yields

$$\begin{aligned}&\left(\cos(\lambda_2 a) - \frac{\lambda_2}{\lambda_1}\sin(\lambda_2 a) - \xi\frac{b_2}{\lambda_2}\left(\sin(\lambda_2 a) + \frac{\lambda_1}{\lambda_2}\cos(\lambda_2 a)\right)\right)(\tau_f - \tau_C|_{x=a}) + \tau_C|_{x=0}\\ &\quad = \frac{\delta_f\tau_f}{\delta_f - \delta_1} - \frac{\xi}{Y_1+Y_2}(1 - (Y_1+Y_2)C_N)M\Big|_{x=0}\\ &\quad\quad - \frac{1}{\lambda_2}\frac{\delta_f}{\delta_f - \delta_1}\left(b_2\xi(1 - \cos(\lambda_2 a)) + \frac{1}{Y_1+Y_2}\sin(\lambda_2 a)\right)\tau_C'\Big|_{x=a}\end{aligned} \tag{44}$$

where $\xi = \frac{\tau_f}{\delta_f - \delta_1}\frac{Y_1}{2K_r}\frac{D_1}{D_1+D_2}(Y_1+Y_2)$. The size of softening zone II, a, can be determined by Eq. (44) for a given applied load. The largest softening zone is reached when

$$\delta|_0 = \delta_f \tag{45}$$

Solving Eqs. (44) and (45) simultaneously, we can find the ultimate load which is defined as the load at which the full debonding will initiate along the interface, as well as the corresponding size of the softening zone.

2.3. Stage III: Elastic-softening-debonding stage

If the load is increased after reaching the debonding limit, full debonding occurs along the interface (Fig. 1 (g)) and propagates a distance d from the location of the flexural crack. In this region, the interface shear stress is zero. Therefore N_1 and N_2 are constants. The stress distribution within region I and II can be obtained by simply shifting d in abscissa in that of elastic-softening stage. Following the same procedure described in the preceding section, we can express the shear stress and axial force in this stage as

Elastic Region I:

$$\begin{aligned}
&\tau = (\tau_f - \tau_C|_{x=a+d})e^{-\lambda_1(x-d-a)} + \tau_C \\
&N_{2e} = N_{2C} + \Delta N_{2e}, \quad \Delta N_{2e} = \frac{b_2(\tau_f - \tau_C|_{x=a+d})}{\lambda_1}e^{-\lambda_1(x-d-a)}
\end{aligned} \tag{46}$$

Softening Region II:

$$\begin{aligned}
\tau &= (\tau_f - \tau_C|_{x=a+d})\left(\cos(\lambda_2(x-d-a)) + \frac{\lambda_2}{\lambda_1}\sin(\lambda_2(x-d-a))\right) \\
&\quad - \frac{b_2}{\lambda_2}\frac{\delta_f}{\delta_f-\delta_1}\tau_C'\Big|_{x=a+d}\sin(\lambda_2(x-d-a)) + \tau_C \\
N_{2S} &= N_{2C} + \Delta N_{2S}, \\
\Delta N_{2S} &= \frac{b_2}{\lambda_2}\left(\sin(\lambda_2(a+d-x)) - \frac{\lambda_2}{\lambda_1}\cos(\lambda_2(a+d-x))\right) + \frac{b_2}{\lambda_2^2}\frac{\delta_f}{\delta_f-\delta_1}(1-\cos(\lambda_2(x-d-a)))\tau_C'|_{x=a}
\end{aligned} \tag{47}$$

Fully debonded region III:

$$\begin{aligned}
&\tau = 0 \\
&N_{2d} = N_{2C} + \Delta N_{2d}, \quad \Delta N_{2d} = N_{2d} - N_{2C} \\
&N_{2d} = N_{2C}|_{x=d} + \frac{b_2}{\lambda_2}\left(\sin(\lambda_2(a+d-x)) - \frac{\lambda_2}{\lambda_1}\cos(\lambda_2(a+d-x))\right) \\
&\qquad + \frac{b_2}{\lambda_2^2}\frac{\delta_f}{\delta_f-\delta_1}(1-\cos(\lambda_2(x-d-a)))\tau_C'\Big|_{x=a}
\end{aligned} \tag{48}$$

Considering the slip in this region, we have

$$\begin{aligned}
\delta &= \delta|_0 + \int_0^x (u_1' - Y_1 w_1'' - u_2'' - Y_2 w_2'')\,dx \\
&= \delta|_{x=0} + \int_0^x \left(-\frac{N_2}{C_1} - \frac{N_2}{C_2} + \frac{Y_1+Y_2}{(D_1+D_2)}(M - (Y_1+Y_2)N_2)\right)dx \\
&= \frac{Y_1}{2K_r}M_1\Big|_{x=o} - \left(\frac{1}{C_1} + \frac{1}{C_2} + \frac{(Y_1+Y_2)^2}{(D_1+D_2)}\right)N_2 x + \frac{Y_1+Y_2}{(D_1+D_2)}\int_0^x M\,dx
\end{aligned} \tag{49}$$

Using above equation and considering Eq. (45), we can determine the softening zone size and ultimate load at this stage as described in the stage II.

3. Deflection of the concrete beam

The deflection of the plated beam can be obtained by integrating Eq. (12) twice:

$$w_1' = w_1'|_{x=0} + \int_0^x \left(-\frac{M}{D_1+D_2} + (Y_1+Y_2)N_{2C}\right)\mathrm{d}x + (Y_1+Y_2)\int_0^x \Delta N_2\,\mathrm{d}x = w_1'|_{x=0} + w_{1C}' + \Delta w_1' \tag{50}$$

where

$$w_{1C}' = \int_0^x \left(-\frac{M}{D_1+D_2} + (Y_1+Y_2)N_{2C}\right)\mathrm{d}x, \quad \Delta w_1' = (Y_1+Y_2)\int_0^x \Delta N_2\,\mathrm{d}x \tag{51}$$

The deflection of the concrete beam is then obtained as

$$w_1 = w_1|_{x=0} + \int_0^x \left(w_1'|_{x=0} + w_{1C}' + \Delta w_1'\right)\mathrm{d}x \tag{52}$$

At $x = L/2$, we have

$$w_1|_{x=L/2} = w_1|_{x=0} + \frac{L}{2}w_1'\Big|_{x=0} + \int_0^{L/2} w_{1C}'\,\mathrm{d}x + \int_0^{L/2} \Delta w_1'\,\mathrm{d}x = 0 \tag{53}$$

Therefore, the mid-span deflection is obtained as

$$w_1|_{x=0} = w_{1C}|_{x=0} + \Delta w_1|_{x=0} \tag{54}$$

Eq. (54) suggests that the concrete beam deflection at the mid-span consists of two parts, i.e., one from the composite beam deformation assuming perfect bonding between the FRP plate and concrete beam and no crack existing in the concrete beam, as given by

$$w_{1C}|_{x=0} = -\int_0^{L/2} w_{1C}'\,\mathrm{d}x \tag{55}$$

And the second part is due to the crack opening and the slip along the FRP–concrete interface, as given by

$$\Delta w_1|_{x=0} = -\frac{L}{2}w_1'\Big|_{x=0} - \int_0^{L/2} w_1'\,\mathrm{d}x = \frac{L}{2}\frac{M_1|_{x=0}}{2K_\mathrm{r}} - \frac{Y_1+Y_2}{(D_1+D_2)}\int_0^{L/2}\int_0^x \Delta N_2\,\mathrm{d}x\,\mathrm{d}x \tag{56}$$

4. Analysis of a simply supported beam under mid-span point load

To demonstrate the strength of the proposed CZM and shed new light on IC debonding, a simply supported beam under a mid-span point load P (Fig. 1) is studied in this section.

4.1. Closed-form solution

Considering a point load P applied at the mid-span of the simply supported beam shown in Fig. 1(a), bending moment and its first and second derivatives are

$$M = \frac{P}{2}\left(\frac{L}{2} - x\right), \quad M' = -\frac{P}{2}, \quad M'' = 0 \tag{57}$$

If P is small, the interface is in elastic stage and the interface shear stress is given by Eqs. (15) and (26) as

$$\tau = \frac{\frac{\tau_\mathrm{f}}{\delta_1}\frac{Y_1}{2K_\mathrm{r}}\frac{D_1}{D_1+D_2}(1+(Y_1+Y_2)b_2C_\tau)\frac{L}{4} + \frac{C_\tau}{2}}{1+\frac{\tau_\mathrm{f}}{\delta_1}\frac{Y_1}{2K_\mathrm{r}}\frac{D_1}{D_1+D_2}(Y_1+Y_2)\frac{b_2}{\lambda_1}} P\mathrm{e}^{-\lambda_1 x} - C_\tau\frac{P}{2} \tag{58}$$

P_e can be calculated by substituting Eq. (58) into Eq. (27) as

$$P_e = \frac{\left(1+\frac{\tau_f}{\delta_1}\frac{h_1}{4K_r}\frac{D_1}{D_1+D_2}\frac{h_1+h_2}{2}\frac{b_2}{\lambda_1}\right)\delta_1}{\frac{\tau_f}{\delta_1}\frac{h_1}{4K_r}\frac{D_1}{D_1+D_2}\left(1-\frac{h_1+h_2}{2}\left(\frac{C_N}{2}+\frac{C_\tau b_2}{\lambda_1}\right)\right)} \tag{59}$$

Note that P_e is the maximum value of load applied to the beam without causing softening in the FRP–concrete interface and therefore is referred to as elastic limit of the FRP–concrete interface in this study. Eq. (59) shows that the P_e is determined by δ_1 and τ_f, as well as the geometry of beams. At this stage, the mid-span deflection due to the flexural crack and interface slip is obtained as

$$\Delta w_1|_{x=0} = -\frac{Y_1+Y_2}{(D_1+D_2)}\frac{Ab_2}{\lambda_1^2}\left(\frac{L_1}{2}-\frac{1}{\lambda_1}\right)+\frac{L}{2}\frac{1}{2K_r} \times \frac{D_1}{D_1+D_2}\left((1+(Y_1+Y_2)b_2C_\tau)M|_{x=0}-(Y_1+Y_2)\frac{Ab_2}{\lambda_1}\right) \tag{60}$$

When $P > P_e$, the FRP–concrete interface enters the elastic-softening stage in which shear stresses in region I (elastic) and II (softening) read:

$$\tau = \left(\tau_f + C_\tau\frac{P}{2}\right)e^{-\lambda_1(x-a)} - C_\tau\frac{P}{2} \quad (x > a) \tag{61}$$

$$\tau = \left(\tau_f + C_\tau\frac{P}{2}\right)\left(\cos(\lambda_2(x-a)) + \frac{\lambda_2}{\lambda_1}\sin(\lambda_2(x-a))\right) - C_\tau\frac{P}{2} \quad (x \leqslant a) \tag{62}$$

This stage ends when the full dobonding begins to initiate. The corresponding load P at this point is referred to as ultimate load of the beam P_u and can be determined from Eq. (62) as

$$P_u = \frac{\left(\cos(\lambda_2 a_u) - \frac{\lambda_2}{\lambda_1}\sin(\lambda_2 a_u)\right)}{-C_\tau\left(\cos(\lambda_2 a_u) - \frac{\lambda_2}{\lambda_1}\sin(\lambda_2 a_u) - 1\right)}\tau_f \tag{63}$$

where a_u is the ultimate softening zone size of the interface determined by Eqs. (44) and (63). According to Eq. (56), the mid-span deflection due to the flexural crack and IC debonding reads

$$\Delta w_1|_{x=0} = -\frac{(Y_1+Y_2)\left(\tau_f+\frac{C_\tau}{2}P\right)b_2}{(D_1+D_2)}\left\{\left(\frac{L_1}{2}-a-\frac{1}{\lambda_1}\right)\left(\frac{1}{\lambda_1}+\frac{1}{\lambda_2}\right)-\frac{1}{\lambda_1\lambda_2^2}\left(-1+\frac{L_1}{2}\lambda_1\right)\cos(\lambda_2 a)+\frac{b_2}{\lambda_1\lambda_2^2}\left(\lambda_2^2\frac{L_1}{2}+\lambda_1\right)\sin(\lambda_2 a)\right\} + \frac{L}{2}\frac{1}{2K_r}\frac{D_1}{D_1+D_2}\left\{\frac{PL}{4}+\frac{Y_1+Y_2}{2}b_2C_\tau\left(\frac{L}{2}-a\right)P-\frac{Y_1+Y_2}{(D_1+D_2)}\frac{\left(\tau_f+\frac{C_\tau}{2}P\right)b_2}{\lambda_2}\left(\sin(\lambda_2 a)+\frac{\lambda_2}{\lambda_1}\cos(\lambda_2 a)\right)\right\} \tag{64}$$

After full debonding initiates, FRP–concrete interface enters the elastic-softening-debonding stage

$$\tau = 0 \quad (x \leqslant d) \tag{65}$$

$$\tau = \left(\tau_f + C_\tau\frac{P}{2}\right)\left(\cos(\lambda_2(x-d-a)) - \frac{\lambda_2}{\lambda_1}\sin(\lambda_2(x-d-a))\right) - C_\tau\frac{P}{2} \quad (d < x \leqslant d+a) \tag{66}$$

$$\tau = \left(\tau_f + C_\tau\frac{P}{2}\right)e^{-\lambda_1(x-d-a)} - C_\tau\frac{P}{2} \quad (x > d+a) \tag{67}$$

At this stage, we have

$$\Delta w_1|_{x=0} = \frac{b_2C_\tau d^2P(3L_1-2d)}{24(D_1+D_2)} - \frac{(Y_1+Y_2)(\tau_f-\tau_C|_{x=d+a})b_2}{(D_1+D_2)}\left\{\left(\frac{L_1}{2}-a-\frac{1}{\lambda_1}\right)\left(\frac{1}{\lambda_1}+\frac{1}{\lambda_2}\right)-\frac{1}{\lambda_1\lambda_2^2}\left(-1+\frac{L_1}{2}\lambda_1 + \frac{d^2}{2}\lambda_2^2 - d\left(\lambda_1+\frac{L_1}{2}\lambda_2^2\right)\right)\cos(\lambda_2 a)+\frac{b_2}{\lambda_1\lambda_2^2}\left(\lambda_2^2\left(\frac{L_1}{2}-d\right)+\lambda_1\left(1-\frac{d^2\lambda_2^2}{2}+\frac{dL_1}{2}\lambda_2^2\right)\right)\sin(\lambda_2 a)\right\} + \frac{L}{2}\frac{1}{2K_r}\frac{D_1}{D_1+D_2}\left\{M|_{x=0}+(Y_1+Y_2)b_2C_\tau M|_{x=d}-\frac{Y_1+Y_2}{(D_1+D_2)}\frac{(\tau_f-\tau_C|_{x=d+a})b_2}{\lambda_2}\left(\sin(\lambda_2 a)+\frac{\lambda_2}{\lambda_1}\cos(\lambda_2 a)\right)\right\} \tag{68}$$

The maximum size of softening zone a_u and ultimate load P_u for a given full debonding distance d can be determined in the same way as in the elastic-softening stage.

4.2. Numerical verification

In this section, numerical examples and parametric studies are conducted for the simply supported beam shown in Fig. 1(a). Same parameters as Wu and Yin (2003) are used: $E_1 = 25$ GPa, $L = 750$ mm, $L_1 = 700$ mm, $h_1 = 150$ mm, $E_2 = 230$ GPa, $b_1 = 100$ mm, $b_2 = 100$ mm, $h_2 = h_{20} = 0.11$ mm. The bi-linear bond-slip parameters are chosen as: $\tau_f = \tau_{f0} = 1.8$ MPa, $K_b = K_{b0} = 160$ M/mm, $G_f = G_{f0} = 0.5$ N/mm.

As verification, the interfacial shear stress and FRP stress calculated by the present analytical solutions are compared with numerical solutions of finite element analysis (FEA) (Wu and Yin, 2003) and presented in Fig. 3. The coefficient of rotational spring c is approximately chosen as 0.0001167. Despite small deviation which may be attributed to the approximation of c value, Fig. 3 shows the present analytical model has achieved good agreements with FEM, which validates the solution of this study.

4.3. Parametric studies

4.3.1. Interfacial shear stress and debonding growth

Interfacial shear stress distributions along the FRP–concrete interface under different loads are illustrated in Fig. 4(a). When $P = 1.05$ KN, the interface is in elastic stage and the shear stress distribution along the FRP–concrete interface is given by Line 1 of Fig. 4(a). A stress concentration exists and the shear stress reaches its maximum at the location of the flexural crack. Noting that the maximum shear stress reaches τ_f

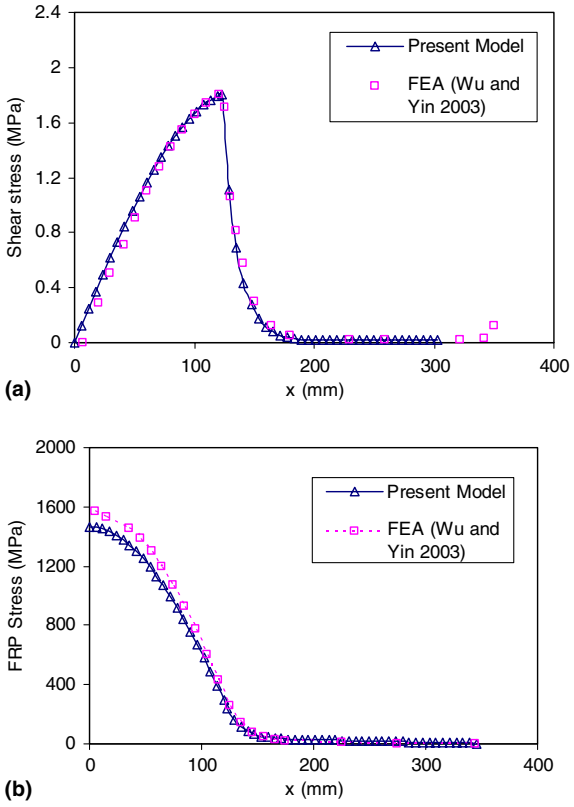

Fig. 3. Comparison between the present solution and FEA (Wu and Yin, 2003): (a) shear stress distribution along the interface; (b) FRP stress distribution.

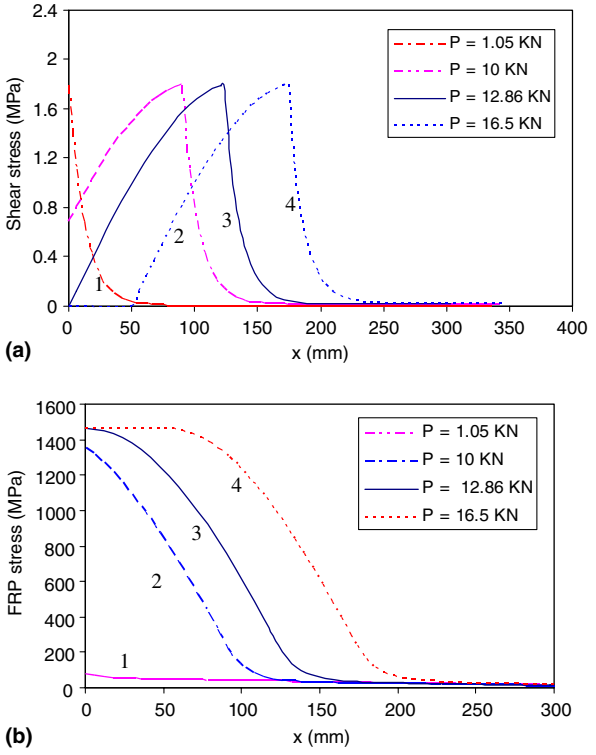

Fig. 4. Interfacial shear stress and FRP stress distributions along FRP–concrete interface under different loads: (a) interfacial shear stress distribution; and (b) FRP stress distribution.

under this load, $P = 1.05$ KN is the elastic limit of the FPR-concrete interface. Softening zone begins to initiate and propagate and the interface enters elastic-softening stage if P is increased further as presented by Line 2 in Fig. 4(a). In this case, $P = 10$ KN and a softening zone with a size of 90.3 mm is formed along the FRP–concrete interface. The size of softening zone increases with P until the full debonding initiates at the location of the flexural crack as shown by Line 3 in Fig. 4(a), of which $P = P_u = 12.86$ KN. The interface debonding grows along the interface with P and a fully debonded region is created as shown by Line 4 in Fig. 4(a). In such a case, $P = 16.5$ KN and a 50 mm fully debonded region has been induced as indicated by the zero shear stress zone in Fig. 4(a). The stress distributions in the FRP plate corresponding to these loads are presented in Fig. 4(b).

The feature of debonding growth along the interface is captured in Fig. 5. Fig. 5(a) shows that the softening zone size a increases with the propagation of debonding. But the increment rate is very small and can be neglected. Therefore, it can be said roughly that the softening zone size is a constant during the debonding growing along the interface. Fig. 5(b) clearly shows that P_u increases with the debonding region size d. Such a trend suggests that P must be increased in order to further debond the interface. Otherwise, the interface debonding tends to arrest. Therefore, for the thicknesses of FRP plates examined in Fig. 5(b), the debonding process is stable, which is also revealed by Rabinovitch and Frostig (2001) in their linearly elastic analysis. With the increment of the debonded region, the moment applied to the concrete beam at the location of the crack, M_{10}, also increases as demonstrated in Fig. 5(c). In this figure, M_{10} is given by

$$M_{10} = \frac{D_1}{D_1 + D_2}\left(\frac{P_u L}{4} + (Y_1 + Y_2) b_2 C_\tau \left(\frac{L}{2} - d\right) P_u - (Y_1 + Y_2)\left(\tau_f + \frac{P C_\tau}{2}\right)\frac{b_2}{\lambda_2}\left(\sin(\lambda_2 a) + \frac{\lambda_2}{\lambda_1}\cos(\lambda_2 a)\right)\right) \tag{69}$$

The stress intensity factor (SIF) at the tip of the flexural crack is proportional to M_{10}. Once M_{10} is big enough such that the SIF of the crack is greater than the critical value of the concrete (fracture toughness

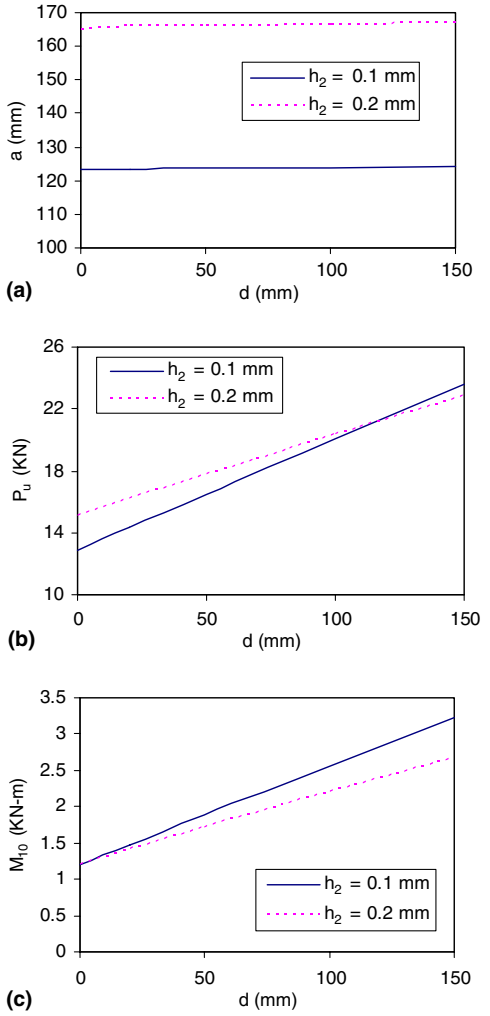

Fig. 5. Debonding propagation along the FRP–concrete interface: (a) softening zone size varies with debonding distance d; (b) ultimate load q_u varies with debonding distance d; (c) M_{10} varies with debonding distance.

of concrete), the flexural crack will initiate again and grow from the depth a_1 to a new depth a_2 in the concrete beam. In such a case, the new P_u of the crack depth a_2 is lower than P which is the P_u for the shorter depth a_1. As a result, IC debonding initiates and grows suddenly and d becomes larger until a new balance between P_u and d is reached for the crack depth a_2. Such a debonding process is unstable and observed frequently in experiments.

4.3.2. Effect of stiffnesses of FRP plates

The stiffness of the FPR plate has been identified by many researchers as an important factor affecting the interfacial stress distribution. In this study, different stiffnesses of FRP plates are modeled by varying the thickness FRP plate as shown in Fig. 6. In Fig. 6(a), shear stress distributions along the FRP–concrete interface for three thicknesses are examined under $P = 12.86$ KN. Obviously, the FRP plate stiffness plays a significant role in the interfacial shear stress distribution and debonding growth. In the case of the FRP plate with the lowest stiffness ($h_2 = 0.11$ mm), a full softening zone is created and full dobonding is initiated as indicated by the zero shear stress at the location of the flexural crack. When $h_2 = 0.2$ mm, the shear stress at the location of the flexural crack is greater than zero, and therefore, only a partial softening zone (79.18 mm) is created along the FRP–concrete interface (Fig. 6(a)). If $h_2 = 0.4$ mm, an even smaller

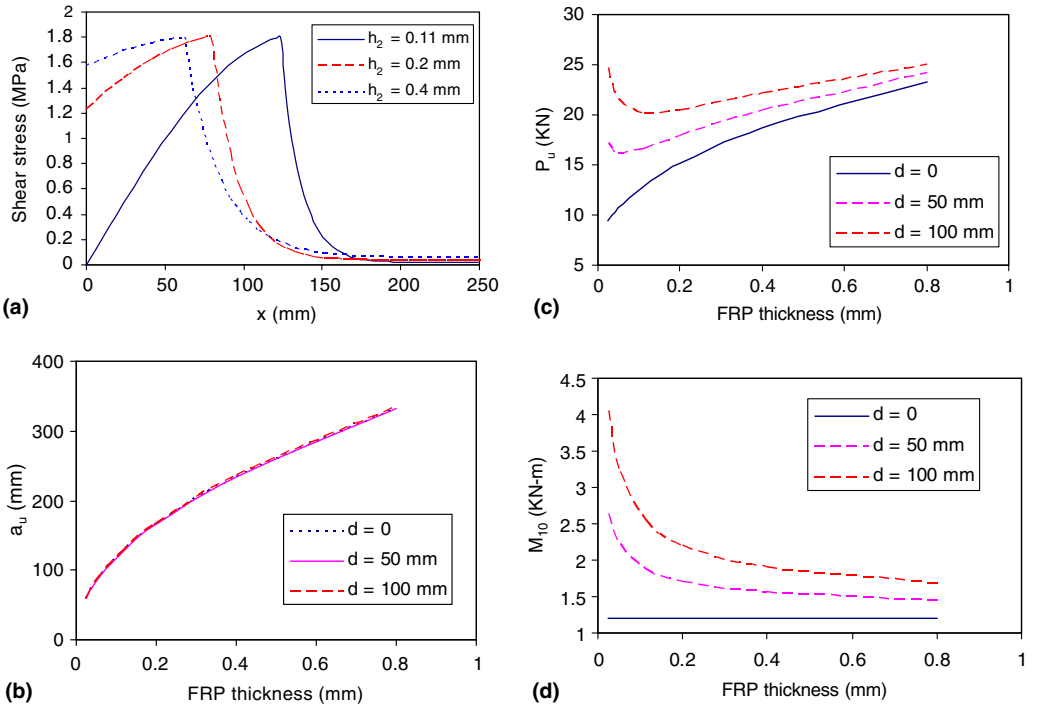

Fig. 6. Effect of FRP plate thickness on debonding: (a) shear stress distribution varies with the FRP plate thickness; (b) softening zone size a varies with the FRP plate thickness; (c) q_u varies with the FRP plate thickness; (d) M_{10} varies the FRP plate thickness.

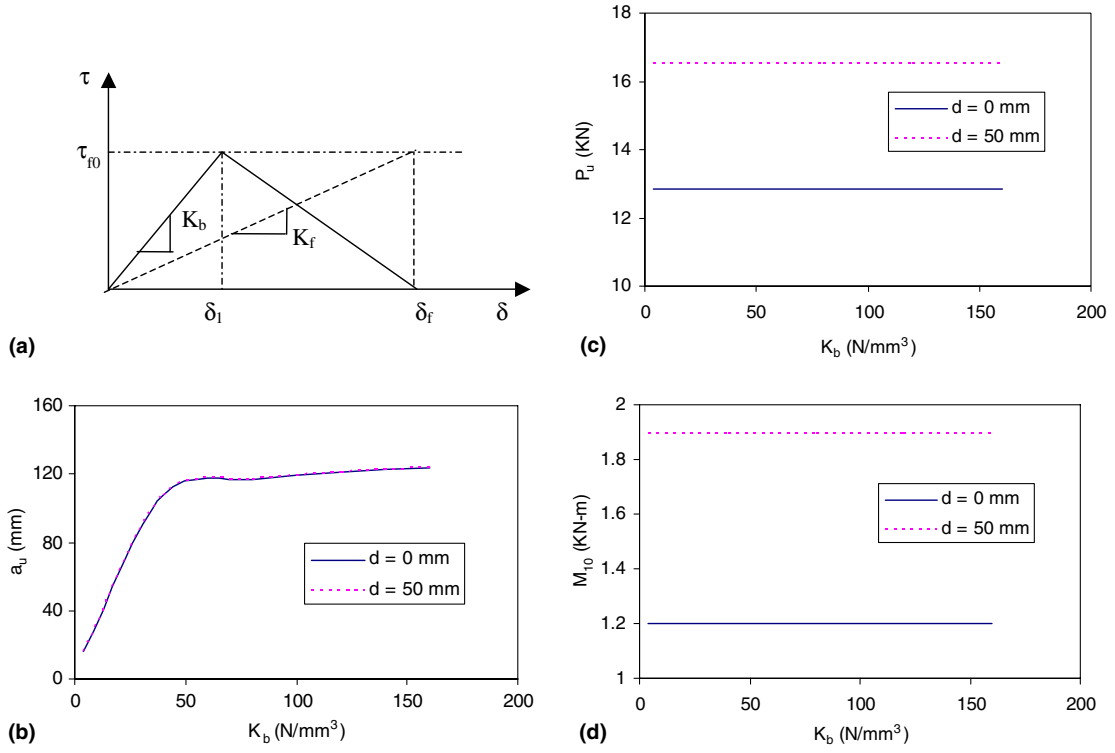

Fig. 7. Effect of K_0 on interfacial debonding: (a) bond-slip shapes with different $\delta_1(K_0)$ considered; (b) softening zone size a varies bond-slip shape parameter k; (c) q_u varies with bond-slip shape parameter k; (d) M_{10} varies with bond-slip shape parameter k.

softening zone (61.86 mm) is observed from Fig. 6(a). Generally, the ultimate softening zone size a_u increases with the thickness of FRP plate as shown in Fig. 6(b). The effect of h_2 on the value of P_u is presented by Fig. 6(c), in which two different trends of P_u varying with h_2 can be observed. When d is very small, P_u increases monotonically with h_2; while after d is greater than a certain value, P_u turns to decrease with h_2 initially until it reaches a minimum value, and then increases with h_2. Fig. 6(d) shows the effect of h_2 on M_{10}. Generally ($d > 0$ in this case), the thicker the FRP plate is, the less the M_{10} is. However, when $d = 0$, a very interesting phenomenon is revealed by Fig. 6(d), i.e., M_{10} is almost a constant regardless the thickness of the FPR plate.

4.3.3. Effect of the bond-slip shape

As aforementioned, the bond-slip law is essentially the constitutive law of the cohesive zone. Currently, many researchers have assumed that two independent parameters (G_f and either τ_f or δ_f) are sufficient to model interfaces using CZM (Rahulkumar et al., 2000; Mohammed and Liechti, 2000; Hutchinson and Evans, 2000). Such an assumption leads to a "two-parameter" nonlinear fracture model which is favorable to experimental characterization of concrete-FRP interfaces. However, recent studies (Chandra et al., 2002; Alfano, in press) show that the CZM shape also plays a significant role in debonding due to different boundary conditions involved. In this section, the sensitivity of the bond-slip shape is examined.

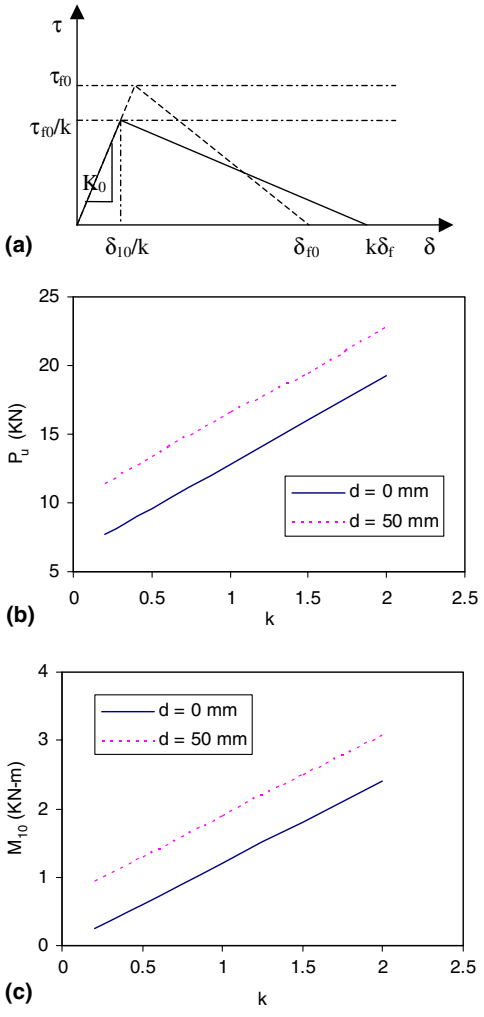

Fig. 8. Bond-slip shape effect (δ_f effect) on debonding: (a) different bond-slip shape with δ_f; (b) P_u varies with δ_f; (c) M_{10} varies with δ_f.

In Fig. 7, the effect of initial stiffness of the bond-slip law K_b on IC debonding is studied. The variation of the bi-linear bond slip shape is achieved by changing the value of δ_1 while keeping all the other parameters same as τ_f, δ_f, and G_f (Fig. 7(a)). Fig. 7(b) shows that the softening zone size increases with K_b. Interestingly, P_u and M_{10} almost do not change with K_b as demonstrated in Fig. 7(c) and (d). In other words, the shape of CZM seems not important in determining the values of P_u and M_{10}. This important feature provides us with an efficient way to calculate P_u and M_{10}. As shown in Fig. 7, to calculate P_u and M_{10}, we can use an assumed linear shape is to replace the real bi-linear bond-slip model (Fig. 7(a)). In this way, the FRP–concrete interface is only in linear elastic stage. In a similar way as described before, we can obtain P_u and M_{10} as

$$P_u = \frac{\delta_f\sqrt{2G_f} + 2FG_f}{R\delta_f + H\sqrt{2G_f}} \tag{70}$$

$$M_{10} = \frac{D_1}{D_1 + D_2}\left(\frac{P_u L}{4} + (Y_1 + Y_2)b_2 C_\tau\left(\frac{L}{2} - d\right)P_u - (Y_1 + Y_2)\left(\tau_f + \frac{P_u C_\tau}{2}\right)\frac{b_2}{\lambda_f}\right) \tag{71}$$

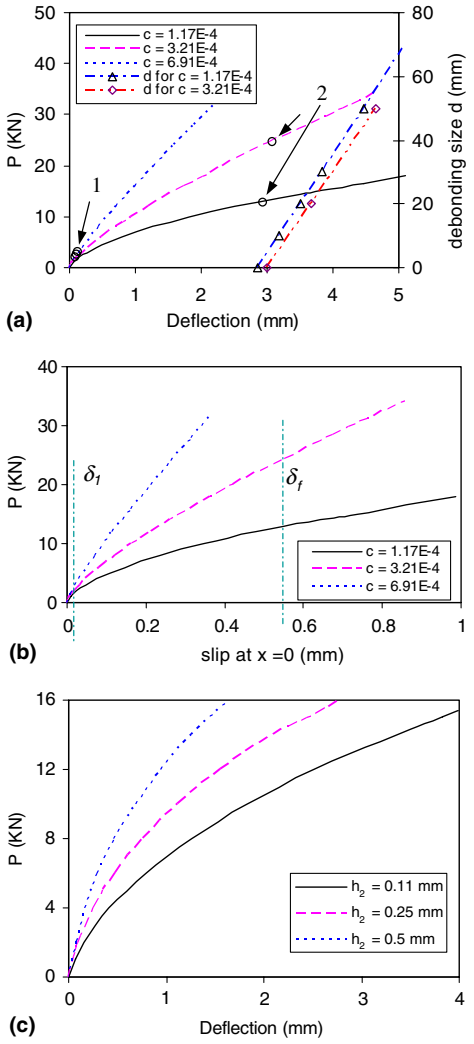

Fig. 9. Load–deflection curve of FRP-plated concrete beam with mid-span crack: (a) effect of flexural crack length; (b) effect of flexural crack length on the slip at $x = 0$; (c) effect of FRP plate thickness.

where

$$H = \frac{Y_1}{2K_r}\frac{D_1}{D_1+D_2}\left(\frac{L}{4}+(Y_1+Y_2)\left(\frac{b_2C_\tau}{2}\left(\frac{L}{2}-d\right)\right)\right)+\frac{Y_1+Y_2}{(D_1+D_2)}\frac{d}{4}(L-d)+\frac{C_d}{2}b_2C_\tau d\left(\frac{L}{2}-d\right),$$

$$R = \frac{Y_1}{2K_r}\frac{D_1}{D_1+D_2}\frac{C_\tau}{2}\frac{b_2}{C_\lambda}-\frac{C_d}{2}\frac{b_2 d}{C_\lambda}, \quad F = \left(\frac{Y_1}{2K_r}\frac{D_1}{D_1+D_2}(Y_1+Y_2)+C_d d\right)\frac{b_2}{C_\lambda},$$

$$C_d = \frac{1}{C_1}+\frac{1}{C_2}+\frac{(Y_1+Y_2)^2}{(D_1+D_2)}, \quad K_f = \frac{\tau_f}{\delta_f} = \frac{2G_f}{\delta_f^2}, \quad \lambda_f = C_\lambda\sqrt{\frac{\tau_f}{\delta_f}}$$

Fig. 8 examines the effect of δ_f (or τ_f) on IC debonding. In this case, δ_f is changing while G_f and initial elastic stiffness K_b are kept as constants as shown in Fig. 8(a). Fig. 8(b) shows that P_u increases monotonically with δ_f. It is obvious that the larger is δ_f, the larger the slip along the FRP–concrete interface can be developed to accommodate the crack opening more easily. As a result, P_u value is increased. As P_u getting larger, M_{10} increases correspondingly as demonstrated in Fig. 8(c).

Fig. 9 presents the curves of the mid-span deflection varying with P. Two particular points are labeled on the curves, i.e., the elastic limit P_e Point 1 and ultimate load P_u Point 2. Initially, load point (mid-span) deflection increases linearly with the applied load P until P_e is reached. After P becomes larger than P_e, the debonding enters its elastic-softening stage. In this stage, the mid-span deflection of the beam increases nonlinearly with P as shown by the segment 1–2 in Fig. 9. Beyond Point 2, the deboding enters elastic-softening-debonding stage, at which the mid-span deflection increases with P almost linearly. Same trend is also observed for the variation of the deflection with the debonding size d. As shown in Fig. 9(a), the mid-span deflection increases almost linearly with the growth of debonding size d. The load-deflection curves of beams with different c values are compared in Fig. 9(a). As mentioned before, c value is related to the flexural crack length, i.e., the larger c value, the smaller cracked length. Fig. 9(a) shows that the flexural crack length has a profound effect on the mid-span deflection and the ultimate load. It is not surprising to see that mid-span deflection increases with crack length a_1 (decreases with c). Similar trend of the interface slip varying with P can be observed as shown in Fig. 9(b). The effect of the FRP plate thickness on the mid-span deflection is demonstrated in Fig. 9(c). In this figure, three different thicknesses are considered to represent three different reinforcement levels. It can be seen that the mid-span deflection can be significantly reduced by using thicker FRP plates.

5. Conclusions

In this study, intermediate crack-induced debonding of FRP-plated concrete beams is studied through a nonlinear fracture mechanics approach. Both the concrete beam and FRP plate are modeled as linearly elastic beams while the FRP–concrete interface is modeled by a bi-linear bond-slip law. A cohesive zone model is thus established and then used to simulate the initiation and growth of FRP–concrete interface debonding. Closed-form solutions of the interfacial stress, the FRP stress and the ultimate load of the plated beam are obtained and verified with a numerical solution based on finite element analysis. Parametric studies are carried out to demonstrate the significant effect of FRP thickness on the interface debonding. The bond-slip shape is examined specifically. In spite of its profound effect on the softening zone size, the bond-slip shape has been found to have little effect on the ultimate load of the FRP-plated beam. From the point of view of CZM, this means that "two-parameter" (G_f, δ_f) model may be sufficient in determining the initiation and growth load of IC debonding. By making use of this unique feature, a simplified explicit expression is obtained, which can be used to determine the ultimate loads of plated concrete beams with flexural cracks conveniently. The cohesive zone model in this study also provides an efficient and effective way to analyze more general FRP–concrete interface debonding.

Acknowledgement

The financial support from ND EPSCoR through NSF grant #EPS-0132289 is gratefully acknowledged.

References

Alfano, G., in press. On the influence of the shape of the interface law on the application of cohesive-zone models. Compos. Sci. Technol.

Barenblatt, G.I., 1962. The mathematical theory of equilibrium cracks in brittle fracture. Adv. Appl. Mech. 7, 55–129.

Bizindavyi, B.L., Neale, K.W., 1999. Transfer Lengths and bond strengths for composites bonded to concrete. J. Compos. Construct. 3, 153–160.

Blackman, B.R.K., Hadavinia, H., Kinloch, A.J., Williams, J.G., 2003. The use of a cohesive zone model to study the fracture of fiber composites and adhesively-bonded joints. Int. J. Fracture 119, 25–46.

Chajes, M.J., Finch Jr., W.W., Januszka, T.F., Thomson Jr., T.A., 1996. Bond and force transfer of composites materials plates bonded to concrete. ACI Struct. J. 93, 209–217.

Chajes, M.J., Januszka, T.F., Mertz, D.R., Thomson Jr., T.A., Finch Jr., W.W., 1995. Shear strengthening of reinforced concrete beams using externally applied composite fabrics. ACI Struct. J. 92, 295–303.

Chandra, N., Li, H., Shet, C., Ghonem, H., 2002. Some issues in the application of cohesive zone models for metal–ceramic interfaces. International Journal of Solids and Structures 39, 2827–2855.

Dai, J., Ueda, T., Sato, Y., 2005. Development of the nonlinear bond stress–slip model of fiber reinforced plastics sheet–concrete interfaces with a simple method. J. Compos. Construct. 9, 52–62.

Dugdale, D.S., 1960. Yielding of steel sheets containing slits. J. Mech. Phys. Solids 8, 100–104.

Hutchinson, J.W., Evans, A.G., 2000. Mechanics of materials: top-down approaches to fracture. Acta Mater. 48, 125–135.

Hutchinson, J.W., Suo, Z., 1992. Mixed mode cracking in layered materials. Adv. Appl. Mech. 29, 63–199.

Lau, K.T., Shi, S.Q., Zhou, L.M., 2001. Estimation of stress intensity factor (KI) for an FRP bonded concrete beam using the superposition method. Mag. Concrete Res. 53, 31–41.

Leung, C.K.Y., 2001. Delamination failure in concrete beams retrofitted with a bonded plate. J. Mater. Civil Eng. 13, 106–113.

Malek, A.M., Saadatmanesh, E.M.R., 1998. Prediction of failure load of R/C beams strengthened with FRP plate due to stress concentration at the plate end. ACI Struct. J. 95, 142–152.

Mohammed, I., Liechti, K.M., 2000. Cohesive zone modeling of crack nucleation at bimaterial corners. J. Mech. Phys. Solids 48, 735–764.

Nakaba, K., Kanakubo, T., Furuta, T., Yoshizawa, H., 2001. Bond behavior between fiber-reinforced polymer laminates and concrete. ACI Struct. J. 98, 359–367.

Neubauer, U., Rostasy, F.S., 1999. Bond failure of concrete fiber reinforced polymer plates at inclined cracks-experimental and fracture mechanics model. In: Dolan, D.W., Rizkalla, S.H., Nanni, A. (Eds.), Proceedings of the Fourth International Symposium. Non-metallic (FRP) Reinforcement for Concrete Structures. Baltimore, USA, pp. 369–382.

Niu, H., Wu, Z., 2005. Numerical analysis of debonding mechanisms in FRP-strengthened RC beams. Comput. Aided Civil Infrastruct. Eng. 20, 354–368.

Paipetis, S.A., Dimarogonas, A.D., 1986. Analytical Methods in Rotor Dynamics. Elsevier Applied Science, London.

Rahulkumar, P., Jagota, A., Bennison, S.J., Saigal, S., 2000. Cohesive element modeling of viscoelastic fracture: application to peel testing of polymers. Int. J. Solids Struct. 37, 1873–1897.

Rasheed, H.A., Pervaiz, S., 2002. Bond slip analysis of fiber-reinforced polymer-strengthened beams. J. Eng. Mech. 128, 78–86.

Roberts, T.M., Haji-Kazemi, H., 1989. Theoretical study of the behavior of reinforced concrete beams strengthened by externally bonded steel plates. In: Proceedings of Institute Civil Engineers, Part 2, London, pp. 39–55.

Rabinovitch, O., Frostig, Y., 2001. Delamination failure of RC beams strengthened with FRP strip—A closed-form high-order and fracture mechanics approach. J. Eng. Mech. 127, 852–861.

Sebastian, W.M., 2001. Significance of midspan debonding failure in FRP-plated concrete beams. J. Struct. Eng. 127, 792–798.

Smith, J.G., Teng, J., 2001. Interfacial stresses in plated beams. Eng. Struct. 23, 857–871.

Taljsten, B., 1996. Strengthening of concrete prisms using the plate bonding technique. Int. J. Fractures 82, 253–266.

Taljsten, B., 1997. Defining anchor lengths of steel and CFRP plates bonded to concrete. Int. J. Adhes. Adhes. 17, 319–327.

Teng, J.G., Smith, S.T., Yao, J., Chen, J.F., 2003. Intermediate crack-induced debonding in RC beams and slabs. Construct. Build. Mater. 17, 447–462.

Triantafillou, T.C., Plevris, N., 1992. Strengthening of RC beams with epoxy-bonded fiber-composite materials. Mater. Struct. 25, 201–211.

Wang, J., Qiao, P., 2004. Interface crack between two shear deformable elastic layers. J. Mech. Phys. Solids 52, 891–905.

Wu, Z., Matsuzaki, T., Tanabe, K., 1997. Interface crack propagation in FRP-strengthened concrete structures. In: Proceedings of the Third International Symposium. Non-Metallic (FRP) Reinforcement for Concrete Structures. Sapporo, Japan, pp. 319–326.

Wu, Z., Yin, J., 2003. Fracture behaviors of FRP-strengthened concrete structures. Eng. Fracture Mech. 70, 1339–1355.

Wu, Z., Yin, J., Ishikawa, T., Iizuka, M., 2002a. Interfacial fracturing and debonding failure modes in FRP-strengthened concrete structures, in: Proceedings of the fourth joint Canada–Japan workshop on composites, Vancouver, Canada, pp. 403–410.

Wu, Z., Yuan, H., Niu, H., 2002b. Stress transfer and fracture propagation in different kinds of adhesive joints. ASCE J. Eng. Mech. 128, 562–573.

Yan, A.M., Marechal, E., Nguyen-Dang, H., 2001. A finite-element model of mixed-mode delamination in laminated composites with an *R*-curve effect. Comput. Sci Technol. 61, 1413–1427.

Yao, J., Teng, J.G., Chen, J.F., 2005. Experimental study on FRP-to-concrete bond joints. Compos. B: Eng. 36, 99–113.

Yuan, H., Teng, J.G., Seracino, R., Wu, Z.S., Yao, J., 2004. Full-range behavior of FRP-to-concrete bonded joints. Eng. Struct. 26, 553–565.

Yuan, H., Wu, Z., Yoshizawa, H., 2001. Theoretical solutions on interfacial stress transfer of externally bonded steel/composite laminates. JSCE J. Struct. Mech. Earthquake Eng. 675, 27–39.